ECS Journal of Solid State Science and Technology

Improving the Electrical and Optical Characteristics of AlGaInP Red Micro-LEDs by Double Dielectric Passivation

To cite this article: Seung-Hyun Mun *et al* 2024 *ECS J. Solid State Sci. Technol.* **13** 026002

ECS Journal of Solid State Science and Technology, 2024 **13** 026002

Improving the Electrical and Optical Characteristics of AlGaInP Red Micro-LEDs by Double Dielectric Passivation

Seung-Hyun Mun,[1] Je-Sung Lee,[1] Sunwoo Shin,[1] Seong Ran Jeon,[2] Soo-Young Choi,[1] Hoe-Min Kwak,[1] Kyung-Pil Kim,[1] Jeongwoon Kim,[1] Chang-Mo Kang,[2,=,z] and Dong-Seon Lee[1,3,=,z]

[1]*School of Electrical Engineering and Computer Science, Gwangju Institute of Science and Technology (GIST), Buk-gu, Gwangju 61005, Republic of Korea*
[2]*Photonic Semiconductor & Display Research Division, Korea Photonics Technology Institute (KOPTI), Gwangju, 61007, Republic of Korea*
[3]*Department of Semiconductor Engineering, Gwangju Institute of Science and Technology (GIST), Buk-gu, Gwangju 61005, Republic of Korea*

This study presents a comprehensive investigation into the optimization of AlGaInP-based red micro-light emitting diodes (LEDs) by implementing double dielectric passivation layers. We employed a two-step passivation process that combined atomic layer deposition (ALD) for a thin Al_2O_3 layer and plasma-enhanced chemical vapor deposition (PECVD) for a thicker dielectric layer to passivate the sidewalls of the LEDs. After double-passivation, the devices exhibited significantly reduced leakage current compared with their non-passivated counterparts. Notably, the passivated LEDs consistently demonstrated lower ideality factors across all size variations. The Al_2O_3-SiN_x passivated devices exhibited a remarkable 38% increase in optical power at a current density of 1000 A cm^{-2}, along with a noteworthy 41% improvement in the external quantum efficiency (EQE) at a current density of 7 A cm^{-2} compared to the reference devices. In addressing the challenge of efficiency degradation in AlGaInP-based red micro-LEDs, this study underscores the effectiveness of dual dielectric passivation, emphasizing the superiority of Al_2O_3-SiN_x as a passivation material. These findings hold promise for micro-LED technology and microdisplays, particularly in applications such as augmented reality by significantly enhancing electrical and optical performance.
 [DOI: 10.1149/2162-8777/ad23ff]

Manuscript submitted October 15, 2023; revised manuscript received January 22, 2024. Published February 7, 2024.

Micro-LEDs have gained significant attention as promising display light sources in recent years because of their numerous advantages, such as high brightness, high contrast, energy efficiency, and long lifespan.[1–4] They are particularly well suited for augmented reality (AR) displays, which demand excellent outdoor visibility and light-weight design. Achieving a pixel density of 5000 pixel per inch or more is crucial for AR displays because of their close viewing distance, necessitating the miniaturization of each red, green, and blue subpixel to approximately 5 μm.[5–7]

However, a critical challenge arises as the size of micro-LEDs decreases: a reduction in external quantum efficiency (EQE).[8–10] Many studies have attributed this phenomenon to dangling bonds of the sidewall surface and plasma-damaged region, leading to increased non-radiative Shockley-Read-Hall (SRH) recombination at the edges of the device.[11–13] AlGaInP-based red LEDs suffer more severe efficiency degradation at smaller sizes compared with InGaN-based blue or green LEDs because of their higher surface recombination velocity.[14,15] The underperformance of red micro-LEDs currently hinders the development of microdisplays, prompting investigations into mitigating efficiency degradation, such as through solution treatment and dielectric film passivation.[16–19]

Commonly employed dielectric materials for passivation layers in LED devices are SiO_2 and SiN_x.[20–22] Among the various methods for depositing dielectric materials, atomic layer deposition (ALD) is highly effective in passivation for micro-LEDs.[23,24] ALD, which is primarily employed for dielectric film passivation, is a process in which vaporized chemicals react with the substrate to coat a thin chemical film along the surface. This process deposits a single layer of thin film in each cycle, allowing precise thickness control, uniformity across large areas, and excellent step coverage.[25–27] Moreover, ALD can be performed at low temperatures, minimizing interference with other layers. Nonetheless, ALD's low deposition rate poses challenges for mass production and cost efficiency because of its single atomic layer accumulation per cycle. To address this, researchers have sought to mitigate the sidewall effect by employing the double-passivation approach, which first deposits a thin layer using ALD and then forms a thick dielectric layer using plasma-enhanced chemical vapor deposition (PECVD). However, most studies have focused on InGaN-based blue or green LEDs, overlooking AlGaInP-based red LEDs.[28–30]

This study presents various sizes of AlGaInP red micro-LEDs with double dielectric passivation layers created via ALD and PECVD, with a focus on performance and mass production considerations. Specifically, Al_2O_3-SiO_2 and Al_2O_3-SiN_x were used as double passivation layers, and their electrical and optical characteristics were thoroughly examined.

Experimental

AlGaInP-based red LED wafers were grown on GaAs substrates via metalorganic chemical vapor deposition (MOCVD). The epi-layers included a sequence of GaInP etching stop layer, n^+-GaInP contact layer, n-AlInP cladding layer, AlGaInP MQWs, p-AlInP cladding layer, p-AlGaInP tensile strain barrier reducing(TSBR) layer, p-GaP window layer, and p^+-GaP contact layer. After the growth of the epitaxial LED structure, the LED mesa was dry-etched using an inductively coupled plasma system. A 300 nm SiO_2 layer was deposited on only one side of the LED mesa for electrical isolation via PECVD. For the n-type electrode, a Pd/Ge/Au (30 nm/30 nm/300 nm) layer was deposited, whereas for the p-type electrode, an AuBe/Au (50 nm/400 nm) layer was used. Both p- and n-type ohmic contacts were obtained by thermal annealing at 250 °C for 30 min in an ambient N_2 atmosphere. Upon completing device fabrication, a double-layer passivation process was employed to reduce sidewall damage. Initially, a 10 nm Al_2O_3 passivation layer was deposited on the entire surface using thermal ALD. Subsequently, a 300 nm SiO_2 or SiN_x layer was deposited as the second passivation layer via PECVD. Finally, the passivation layers on the p-pad and n-pad were removed using reactive-ion etching. The electrical and optical characteristics of the packaged samples

[=]Equal contribution.
[z]E-mail: dslee66@gist.ac.kr; fd1kcm@kopti.re.kr

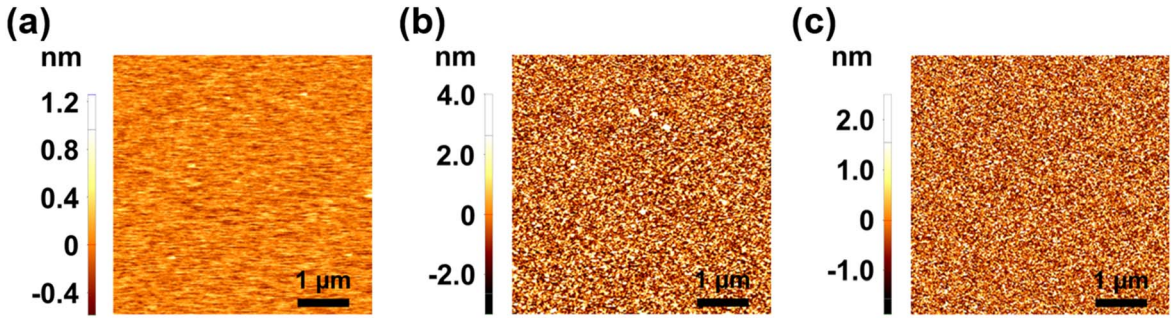

Figure 1. Atomic force microscopy images of the 10-nm-thin film on sapphire: (a) Al_2O_3, (b) SiO_2, and (c) SiN_x.

were measured using an integrating sphere in conjunction with a spectroscope and sourcemeter (Keithley KE2612A).

Results and Discussion

The first passivation layer plays a crucial role in reducing leakage current by filling the dangling bonds on the surface with stable atoms. Therefore, the film quality of the first passivation layer is an important factor in reducing leakage current. To find a suitable material as the first passivation layer, the roughness of 10 nm thick Al_2O_3, SiO_2, and SiN_x thin films was measured using an atomic force microscope (AFM) as shown in Fig. 1. The Al_2O_3 film was deposited using ALD at 150 °C, and the SiO_2 and SiN_x films were deposited using PECVD at 300 °C. The measured root-mean-square values of Al_2O_3, SiO_2, and SiN_x were 0.138, 1.454, and 0.881 nm, respectively. The Al_2O_3 layer appeared as a very uniform film. By contrast, the SiO_2 and SiN_x layers appeared as rough films that could be distinguished by grains. On the basis of the film quality measured by AFM, we selected the Al_2O_3 material as the first passivation layer.

Figure 2 illustrates the fabrication process of the AlGaInP red micro-LED with double-layer passivation. To facilitate direct comparison, a reference LED was initially fabricated using a standard semiconductor process, followed by the application of a double passivation layer across the entire reference LED surface. Subsequently, the passivation layer was removed from the pad to create a passivated LED.

In Fig. 3a, we observe scanning electron microscopy (SEM) images capturing LEDs with different dimensions including 10 × 10 μm^2, 20 × 20 μm^2, 50 × 50 μm^2, and 100 × 100 μm^2. To ensure consistent light-emitting areas regardless of variations in the LED mesa size, we kept the ratio of the SiO_2 layer's insulating area to mesa area and the metal area to mesa area constant at 20%, respectively. In Fig. 3b, we present an image of 10 μm sized AlGaInP LEDs fabricated using the double-layer passivation technique. The passivation layer covers the entire LED surface area except for the pads, as shown. Figure 3c shows a cross-sectional view of the double-passivated LED obtained by SEM. The top layer represents the carbon coating applied during a focused ion beam (FIB). The thicknesses of the SiO_2, p-metal, and double passivation layers were 292, 431, and 308 nm, respectively. Notably, all layers were applied without cutting off on both the LED mesa and the sidewalls of the LED.

Figure 4 shows the current density-voltage characteristics of reference and double-passivated LEDs according to various device sizes. Smaller LEDs exhibited higher leakage currents in the reverse-bias region. Specifically, the 10 μm micro-LED exhibited a reverse current approximately one order of magnitude higher than that of the 100 μm micro-LED, regardless of passivation, which is consistent with previous findings.[9,10]

Figures 5a and 5b show the current density-voltage characteristics of the reference, Al_2O_3 single-passivated, and double-passivated LEDs for device sizes of 10 × 10 and 100 × 100 μm^2, respectively. Under reverse bias, LEDs with a passivation layer exhibited reduced leakage current compared to the reference devices. When the device size was 100 × 100 μm^2, the difference in leakage current between single and double passivation was not significant. However, for the device size of 10 × 10 μm^2, the device with double passivation layers showed better leakage-current characteristics than

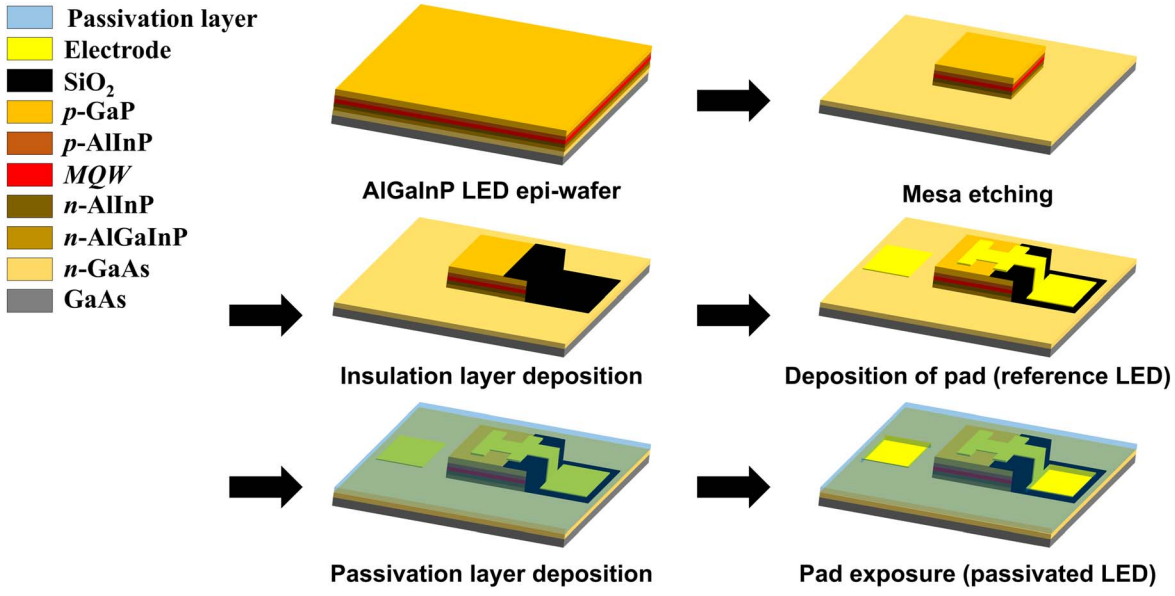

Figure 2. Schematic diagram of the fabrication steps of AlGaInP micro-LED device with double passivation.

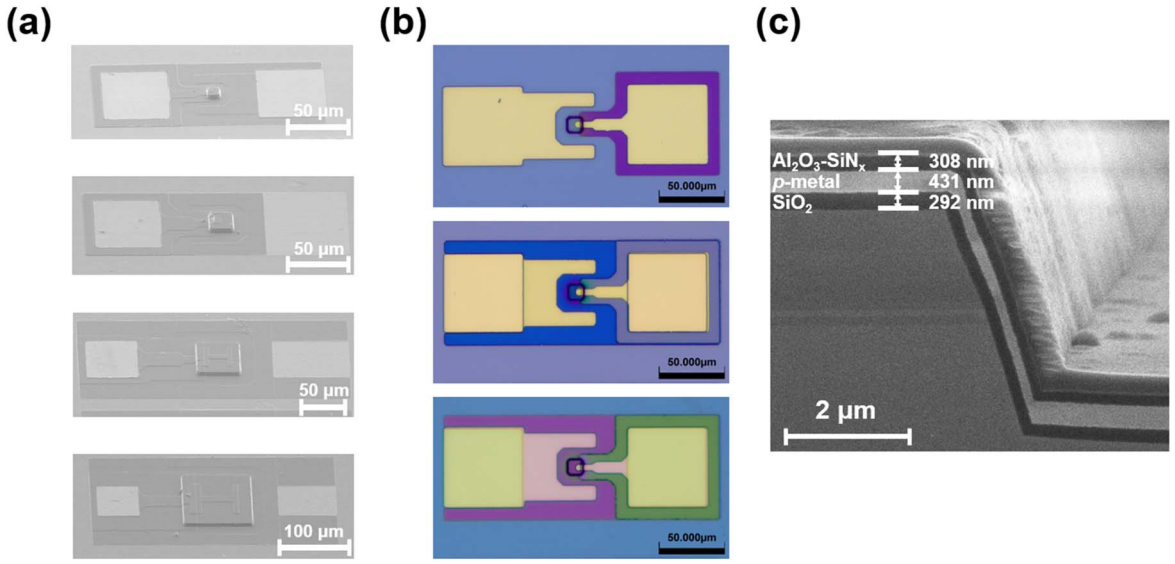

Figure 3. (a) Scanning electron microscope images for different sizes of AlGaInP red micro-LEDs with double passivation and (b) Microscope photograph of reference LED, Al_2O_3+SiO_2 passivated LED, and Al_2O_3+SiN_x passivated LED and (c) Scanning electron microscope images of the double passivation layer.

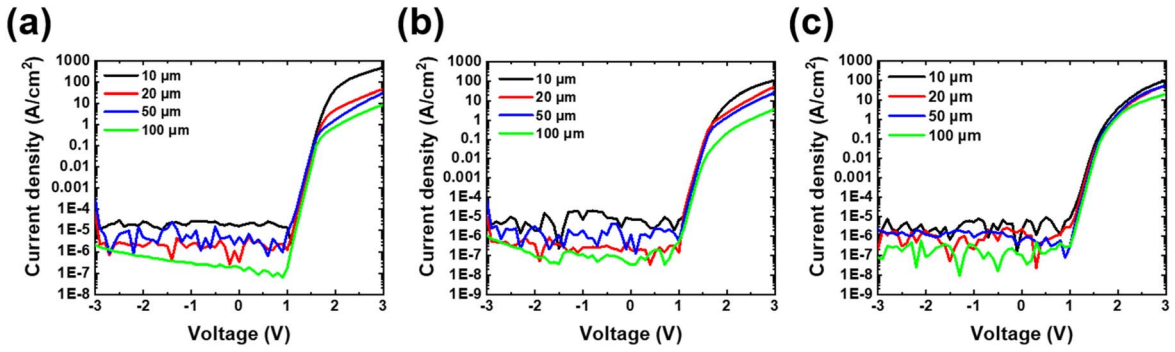

Figure 4. Current density-voltage (J-V) characteristics for different sizes of AlGaInP red micro-LEDs (a) reference, (b) Al_2O_3+SiO_2 passivation, and (c) Al_2O_3+SiN_x passivation.

with the single passivation layer. For the 100 × 100 μm^2 LED, the Al_2O_3-SiO_2 and Al_2O_3-SiN_x LEDs had a leakage current reduction rate of 68.7% and 81.8%, respectively, compared to the reference LED. Further, in the case of the 10 × 10 μm^2 LED, the Al_2O_3-SiO_2 and Al_2O_3-SiN_x LEDs also had a leakage current reduction rate of 57.4% and 83.9%, respectively, compared to the reference LED. Thus, the leakage current reduction rates were similar when applying double passivation, regardless of the chip size. Notably, the SiN_x layer, which has a higher dielectric constant and superior insulating properties,[31,32] is slightly more effective than SiO_2 in reducing leakage current. We believe that the more densely the second layer is deposited, the more it helps the first layer to stably fill the dangling bonds on the surface. Considering the AFM results presented in Fig. 1, it is clear that the best device performances resulted from Al_2O_3-SiN_x passivation layers because the SiN_x layer had better film quality than SiO_2.

Figure 6a shows electroluminescence images according to the passivation layer for a 10 × 10 μm^2 LED device. At a current density of 10 A cm^{-2}, all devices showed similar brightness levels; however, at the lower current densities (1 A cm^{-2}), the Al_2O_3-SiN_x passivated LED demonstrates superior emission compared to the others. Figure 6b illustrates the ideality factor of both the reference and double-passivated LEDs, varying with device size. The ideality factor of LEDs can be determined using the following equation:

$$n = \frac{q}{kT}\left(\frac{\partial \ln I}{\partial V}\right)^{-1} \quad [1]$$

where n represents the ideality factor, q is the electron charge, k is the Boltzmann constant, T is the absolute temperature, I is the forward current, and V is the applied voltage. Generally, an ideality factor close to 2 indicates that the SRH recombination is dominant.[33,34] Across devices of all sizes, the ideality factor falls within the range of 1.8 to 2, regardless of the passivation layer. As the device size decreases below 50 μm, the ideality factor increases because of the higher density of surface states.[11] However, double-layer passivated LEDs exhibit a smaller ideality factor than reference LEDs. This result suggests that double-layer passivation mitigates sidewall defects caused by plasma dry etching.

Figure 7a presents the measurement light output power for 50 μm × 50 μm^2 LEDs with different passivation methods at current densities ranging from 8 to 2400 A cm^{-2}. Due to limitations with our measurement equipment, it was impracticable to measure the light output power for LEDs of smaller dimensions, specifically those measuring 10 μm and 20 μm. Consequently, the analysis was confined to 50 μm LED devices. Both the Al_2O_3-SiO_2 LED and Al_2O_3-SiN_x LED exhibited increased light output power, with gains

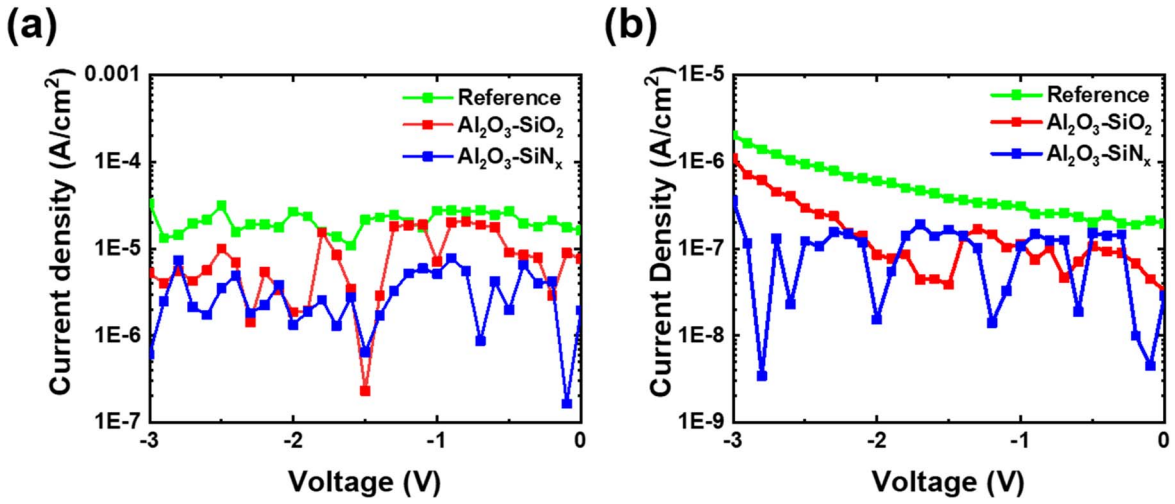

Figure 5. Current density-voltage (J-V) characteristics of (a) 10 × 10 and (b) 100 × 100 μm^2 AlGaInP devices with different passivation.

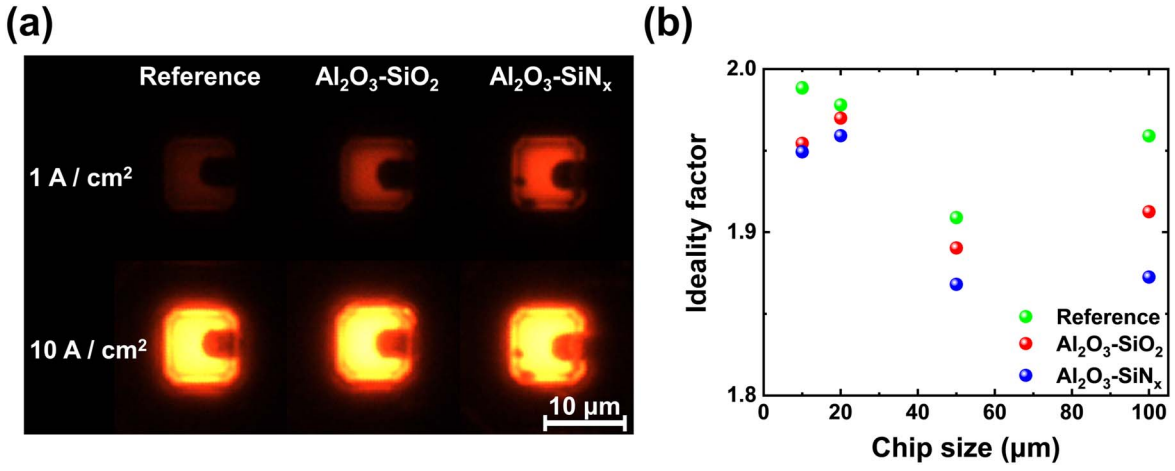

Figure 6. (a) Electroluminescent images of different passivation LED sizes of 10 × 10 μm^2 at current densities of 1 A cm^{-2} and 10 A cm^{-2} (b) Ideality factor of different sizes of AlGaInP micro-LEDs with and without passivation.

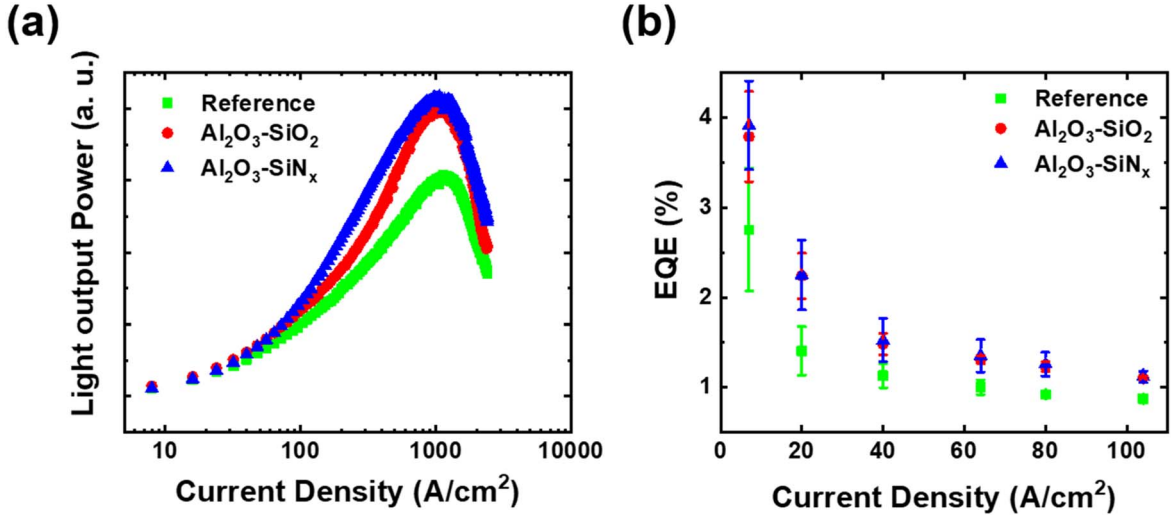

Figure 7. (a) Light output power characteristics of 50 × 50 μm^2 AlGaInP devices with different double passivations (b) EQE performance of 50 × 50 μm^2 AlGaInP devices with and without passivation.

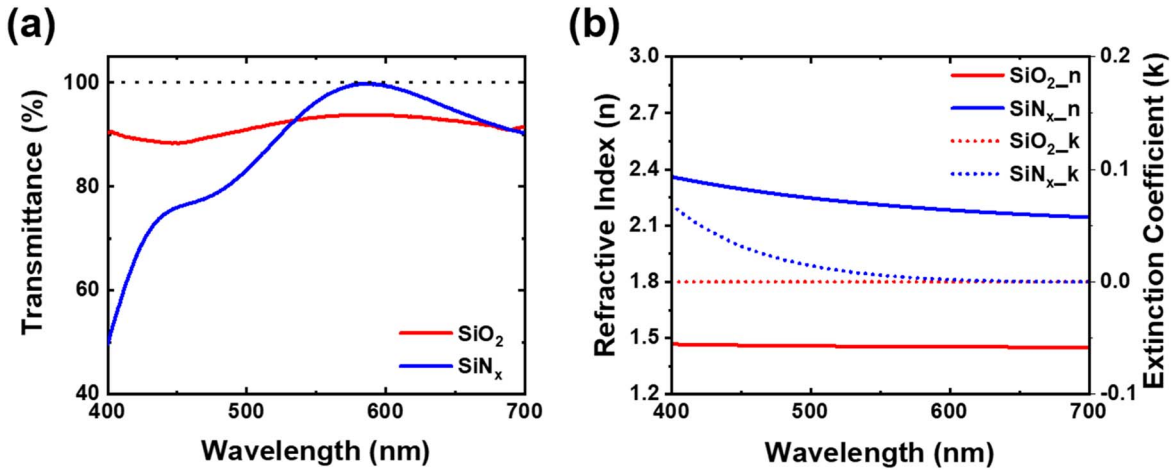

Figure 8. (a) Transmittance of the SiO_2 and SiN_x layer on Al_2O_3 (b) refractive index and extinction coefficient of the SiO_2 and SiN_x.

of 35% and 38%, respectively, compared with the reference LED at a high current density of 1000 A cm^{-2}. The enhanced light output power in the passivated LED appears to result from the improved light extraction efficiency. A more comprehensive explanation of this phenomenon is provided in subsequent sections. Figure 7b shows the EQE as a function of the injection current densities for 50 μm LEDs. Passivated LEDs, whether Al_2O_3-SiO_2 or Al_2O_3-SiN_x LED, demonstrated improved EQE. Specifically, the EQE of the Al_2O_3-SiN_x LED increased by 1.41 times at low current densities (7 A cm^{-2}) and 1.28 times at high current densities (104 A cm^{-2}) compared with the EQE of the reference LED.

To clarify the increase in light output power, we conducted transmittance measurements on two samples: (i) where SiO_2 film was deposited onto Al_2O_3 and (ii) where SiN_x film was deposited onto Al_2O_3 (see Fig. 8a). The transmittance of SiO_2 was 93.3%, while that of SiN_x was 97.3% at 625 nm, which is in proximity to the emission region. SiN_x proves to be a more suitable passivation material in the red spectral region than in the blue and green spectral regions. This preference arises not only from SiN_x's higher transmittance relative to SiO_2 but also from its transmittance declining in the wavelength region below 580 nm.

Next, we measured the refractive indices and extinction coefficients of the two passivation materials using ellipsometry. As depicted in Fig. 8b, the refractive indices of SiO_2 and SiN_x in the emission region were 2.17 and 1.45, respectively. Assuming normal incidence on the interface and loss-free dielectric, given the near-zero extinction coefficients of both materials at an emission wavelength of approximately 625 nm, we can calculate the Fresnel power transmittance using the following equation:[35,36]

$$T = \frac{4n_1n_2}{(n_1 + n_2)^2} \quad [2]$$

where T represents the Fresnel power transmittance, while n_1 and n_2 denote the refractive indices of the passivation layer. Neglecting the multiple reflections at each interface for simplicity, the transmittance of a double passivation layer can be expressed as the product of the transmittance at each interface.[37] In the emission wavelength range, the refractive indices of GaP, Al_2O_3, SiO_2, and SiN_x are 3.3, 1.77, 1.45, and 2.17, respectively. Consequently, the Fresnel power transmittances of the reference LED, Al_2O_3-SiO_2 LED, and Al_2O_3-SiN_x passivated LED were calculated to be 71.3%, 86.9%, and 77.7%, respectively. Notably, the Fresnel power transmittance of the double-passivated LEDs surpassed that of the reference LED. In addition, the Fresnel power transmittance of the Al_2O_3-SiO_2 passivated LED was higher than that of the Al_2O_3-SiN_x passivated LED primarily because of its lower refractive index. Despite the Al_2O_3-SiN_x passivated LED exhibiting lower Fresnel power transmittance than the Al_2O_3-SiO_2 passivated LED, the improved electrical and optical properties appear to reduce the leakage current sufficiently to compensate for the reduced Fresnel power transmittance.

Conclusions

In this study, we successfully fabricated AlGaInP red micro-LEDs with double dielectric passivation using ALD and PECVD. The deposition of this double-passivated layer of micro-LED sidewalls was structurally sound and devoid of cracks, thereby reducing the presence of dangling bonds. Notably, as the LED size decreased, the double passivation effect proved particularly effective in reducing the leakage current than single passivation. Furthermore, regardless of the device size, the ideality factor consistently improved in the double-passivated device, showing enhanced electrical characteristics. Consequently, both light output power and EQE showed significant improvements in the double-passivated LED devices. It is worth mentioning that both the electrical and optical properties of the Al_2O_3-SiN_x passivated LED surpassed those of the Al_2O_3-SiO_2 passivated LEDs, which suggests that SiN_x can serve as an effective passivation layer for red LEDs.

Acknowledgments

This work were supported by the Technology Innovation Program(20017406) funded by the Ministry of Trade, Industry & Energy(MOTIE, Korea) and regional innovation mega project program through the Korea Innovation Foundation funded by Ministry of Science and ICT (2023-DD-UP-0015).

ORCID

Dong-Seon Lee https://orcid.org/0000-0003-2706-8702

References

1. J. Day, J. Li, D. Y. C. Lie, C. Bradford, J. Y. Lin, and H. X. Jiang, *Appl. Phys. Lett.*, **99**, 2 (2011).
2. V. W. Lee, N. Twu, and I. Kymissis, *Inf. Disp.*, **32**, 16 (2016).
3. P. J. Parbrook, B. Corbett, J. Han, T. Y. Seong, and H. Amano, *Laser Photon. Rev.*, **15**, 2000133 (2021).
4. P. Tian, A. Althumali, E. Gu, I. M. Watson, M. D. Dawson, and R. Liu, *Semicond. Sci. and Technol.*, **31**, 045005 (2016).
5. E. H. Virey and N. Baron, *SID Symp. Dig. Tech. Pap.*, **49**, 593 (2018).
6. T. Wu, C.-W. Sher, Y. Lin, C.-F. Lee, S. Liang, Y. Lu, S.-W. Huang Chen, W. Guo, H.-C. Kuo, and Z. Chen, *Appl. Sci.*, **8**, 1557 (2018).
7. T. Zhan, K. Yin, J. Xiong, Z. He, and S.-T. Wu, *iScience*, **23**, 101397 (2020).
8. F. Olivier, S. Tirano, L. Dupré, B. Aventurier, C. Largeron, and F. Templier, *J. Lumin.*, **191**, 112 (2017).
9. J. M. Smith, R. Ley, M. S. Wong, Y. H. Baek, J. H. Kang, C. H. Kim, M. J. Gordon, S. Nakamura, J. S. Speck, and S. P. DenBaars, *Appl. Phys. Lett.*, **116**, 071102 (2020).
10. J. T. Oh et al., *Opt. Express*, **26**, 11194 (2018).
11. F. Olivier, A. Daami, C. Licitra, and F. Templier, *Appl. Phys. Lett.*, **111**, 022104 (2017).

12. J. Kou, C. C. Shen, H. Shao, J. Che, X. Hou, C. Chu, K. Tian, Y. Zhang, Z. H. Zhang, and H. C. Kuo, *Opt. Express*, **27**, 643 (2019).
13. Y. Boussadi, N. Rochat, J.-P. Barnes, B. B. Bakir, P. Ferrandis, B. Masenelli, and C. Licitra, *J. Lumin.*, **234**, 117937 (2021).
14. K. A. Bulashevich and S. Y. Karpov, *Phys. Status Solidi—Rapid Res. Lett.*, **10**, 480 (2016).
15. M. Boroditsky, I. Gontijo, M. Jackson, R. Vrijen, E. Yablonovitch, T. Krauss, C.-C. Cheng, A. Scherer, R. Bhat, and M. Krames, *J. Appl. Phys.*, **87**, 3497 (2000).
16. D. M. Geum, S. K. Kim, C. M. Kang, S. H. Moon, J. Kyhm, J. Han, D. S. Lee, and S. Kim, *Nanoscale*, **11**, 23139 (2019).
17. B. O. Jung, W. Lee, J. Kim, M. Choi, H. Y. Shin, M. Joo, S. Jung, Y. H. Choi, and M. J. Kim, *Sci. Rep.*, **11**, 4535 (2021).
18. H. H. Huang, S. K. Huang, Y. L. Tsai, S. W. Wang, Y. Y. Lee, S. Y. Weng, H. C. Kuo, and C. C. Lin, *Opt. Express*, **28**, 38184 (2020).
19. J. Park, W. Baek, D. M. Geum, and S. Kim, *Nanoscale Res. Lett.*, **17**, 29 (2022).
20. P. Zuo et al., *Opt. Quantum Electron.*, **48**, 288 (2016).
21. V. Sheremet et al., *Superlattices Microstruct.*, **113**, 623 (2018).
22. K. M. Chang, C. C. Lang, and C. C. Cheng, *Phys. Status Solidi A*, **188**, 175 (2001).
23. G. Dingemans, M. C. M. van de Sanden, and W. M. M. Kessels, *Electrochem. Solid-State Lett.*, **13**, H76 (2010).
24. M. S. Wong, D. Hwang, A. I. Alhassan, C. Lee, R. Ley, S. Nakamura, and S. P. DenBaars, *Opt. Express*, **26**, 21324 (2018).
25. R. G. Gordon, D. Hausmann, E. Kim, and J. Shepard, *Chem. Vap. Deposition*, **9**, 73 (2003).
26. K. E. Elers, T. Blomberg, M. Peussa, B. Aitchison, S. Haukka, and S. Marcus, *Chem. Vap. Deposition*, **12**, 13 (2006).
27. H. Kim and I.-K. Oh, *Jpn. J. Appl. Phys.*, **53**, 03DA01 (2014).
28. C.-M. Yang, D.-S. Kim, S.-G. Lee, J.-H. Lee, Y. S. Lee, and J.-H. Lee, *IEEE Electron Device Lett.*, **33**, 564 (2012).
29. R. T. Ley, J. M. Smith, M. S. Wong, T. Margalith, S. Nakamura, S. P. DenBaars, and M. J. Gordon, *Appl. Phys. Lett.*, **116**, 251104 (2020).
30. D.-H. Lee, J.-H. Lee, J.-S. Park, T.-Y. Seong, and H. Amano, *ECS J. Solid State Sci. Technol.*, **9**, 055001 (2020).
31. T. Kikkawa, M. Nagahara, N. Okamoto, Y. Tateno, Y. Yamaguchi, N. Hara, K. Joshin, and P. Asbeck, *IEDM Tech. Dig.*, **25.4.1**, 585 (2001).
32. T. Hashizume, S. Ootomo, T. Inagaki, and H. Hasegawa, *J. Vac. Sci. Technol. B*, **21**, 1828 (2003).
33. C.-T. Sah, R. N. Noyce, and W. Shockley, *Proc. IRE*, **45**, 1228 (1957).
34. J. M. Shah, Y.-L. Li, T. Gessmann, and E. F. Schubert, *J. Appl. Phys.*, **94**, 2627 (2003).
35. E. Hetch, *Optics* (Adison Wesley, San Francisco) 4th ed., p. 121 (2002).
36. H. Weber, *J. Modern Opt.*, **61**, 1219 (2014).
37. U. Sikder and M. A. Zaman, *Opt. Laser Technol.*, **79**, 88 (2016).